Single and Multiple Open-Switch Fault Diagnosis in Electric Drives via Zero-Current Interval Analysis

L. E. Venghi, F. Aguilera, *Senior Member, IEEE,* P. M. de la Barrera, *Senior Member, IEEE,* and C. H. De Angelo, *Senior Member, IEEE*

***Abstract*—In this work, a new and simple method for open-switch fault diagnosis in electric drives based on zero-current detection is proposed. The approach requires only two phase current sensors, with the measured currents being normalized and separated into positive and negative half-cycles. A variable-sample-time moving average is introduced for post-processing the signals. Zero-current interval detection is employed to diagnose both single and multiple open-switch faults. The proposed method was experimentally validated under various fault conditions, including single-switch, crossed-switch, full-leg, and two upper- or lower-switch open-circuit faults. Experimental results demonstrate that, despite its simplicity and ease of implementation, the method reliably detects all single and double open-switch fault scenarios in less than one electrical cycle, across different motor operating conditions.**

Link to graphical and video abstracts, and to code: https://latamt.ieeer9.org/index.php/transactions/article/view/9957

***Index Terms*—Detection and isolation, Electric Drives, Fault Diagnosis, Inverter, Open-Switch Faults.**

I. Introduction

ELECTRIC DRIVES (ED) are composed by a motor, an inverter, a control system, and a set of sensors. In particular, faults in inverter switches are 31% of the total faults in industry [1], [2]. These faults are typically classified as short-circuit (SC) or open-circuit (OC) faults.

SC faults may occur due to unclamped inductive switching, high-temperature latch-up, second breakdown, or energy shocks [3]. These faults produce instantaneous overcurrents, which can cause damage to other components of the inverter [4]. Consequently, hardware protection circuits based on the desaturation detection method, the di/dt feedback method, the gate voltage method, and the slow shutdown were proposed [5].

OC faults occur as a result of various factors, including aging and accumulation of damage due to stress factors (overcurrent, temperature, vibration and humidity), or gate driver failures [3]. As a consequence of OC faults, phase currents do not flow through the affected switches. This effect causes an overload in the remaining power devices, which in the long term implies secondary faults in the inverter and even a total shutdown of the ED. For this reason, fault detection and isolation (FDI) strategies are used in inverter switches to prevent extensive damage to the ED. These FDI strategies can be classified into model-based, expert knowledge-based, and signal-based [6].

Model-based FDI strategies rely on the mathematical modeling of the ED to estimate currents or voltages and compare them with the measured values in order to generate residuals. Several model-based estimation strategies were proposed to develop OC FDI, such as Luenberger's observer [7], sliding-mode observer [8], Kalman filter [9], among others. The main characteristic of these strategies is their ability to rapidly detect faults in real-time implementations without requiring additional hardware, as they rely on estimations. However, the diagnostic performance strongly depends on the accuracy of the model and its parameters.

Expert-knowledge-based strategies comprise a set of rules derived from a database. These strategies include fuzzy logic [10], decision trees [11], support vector machines [12], and neural networks [13]. The main drawback of knowledge-based strategies is their requirement for a substantial number of fault tests to adequately train the algorithm, thereby limiting their implementation.

Signal-based strategies utilize signals from the control strategy to develop indexes for fault diagnosis by identifying failures in the operating condition of the ED. In addition, they can be classified according to the signals used for the diagnosis: voltage-based or current-based. The voltage-based diagnostic residuals are derived from switching node voltages [14], instant voltage difference at the extremes of an arm [15], or gate voltages [16]. These strategies have a fast detection speed, but require additional hardware, increasing their cost.

In contrast, current-based approaches can take advantage of current sensors already present in the ED to implement motor control, so they can be considered a low-cost solution. Among these strategies, in [17] a FDI strategy based on the Park transformation is proposed for multiple OC faults in induction motor (IM) drives using two current sensors. This strategy detects faults by analyzing the time in which the phase current vector remains in each sector of a stationary reference frame. Then, the faults are isolated on the basis of the average values of the normalized line-to-line currents. However, this

The associate editor coordinating the review of this manuscript and approving it for publication was Diego Rivelino Espinoza Trejo (*Corresponding author: Luis Esteban Venghi*).

This work was supported by Consejo Nacional de Investigaciones Científicas y Técnicas, Universidad Nacional de Rafaela and Universidad Nacional de Río Cuarto.

Luis Esteban Venghi is with the Centro de Investigación y Transferencia, Rafaela, Santa Fe, Argentina (e-mail: luisesteban.venghi@unraf.edu.ar).

F. Aguilera, P. M. de la Barrera, and C. H. De Angelo are with Grupo de Electrónica Aplicada, Instituto de Investigaciones en Tecnologías Energéticas y Materiales Avanzados, Córdoba, Argentina (e-mails: faguilera@ing.unrc.edu.ar, pbarrera@ing.unrc.edu.ar, and cdeangelo@ing.unrc.edu.ar).

FDI is based on the comparison of the reference current against the measured current, making the strategy dependent on the performance of the control strategy. In [18] two normalized diagnostic variables are introduced, one of them based on the slope of the current vector in the stationary reference frame and the other on the average values of normalized line currents. The information is combined to perform the FDI strategy in multiple inverter switches of an IM drive. However, the robustness of the strategy depends on a sampling window that varies in each cycle according to the angular velocity, making its implementation challenging in variable-speed ED. In [19] a FDI strategy for variable-speed drives is proposed, based on the analysis and pattern recognition of stator currents. First, an OC fault is detected by comparing the average phase current values with a predefined threshold. Then, a trajectory analysis is conducted using a histogram from the current vector angle. The fault is identified by comparing the obtained signature with a database of known fault signatures. Although this strategy can diagnose multiple OC faults, its effectiveness depends on the theoretical signature database. Thus, for full-leg faults, the study is limited to analytical detection and isolation, without experimental demonstration. In [20] a FDI detects changes in the slope of the trend lines of the current vector trajectories to diagnose multiple inverter OC faults. The construction of these trend lines depends on the operating frequency; therefore, it is not practical to implement them in variable-speed ED, where current patterns change significantly, making it difficult to establish consistent trend lines. In addition, this proposal was only validated at a rated frequency. A standard approach to implementing OC FDI is based on averaging the phase current over a cycle. For example, in [21], the use of normalized average current and adaptive thresholds is proposed to detect and isolate multiple OC faults in PMSM drives. Nonetheless, achieving the desired performance requires additional computing resources to dynamically adjust thresholds and tuning the cutoff frequency of low-pass filters. Furthermore, as with other strategies based on the evaluation of current cycles, it encounters difficulties in effectively discriminating between full-leg faults and normal operating conditions, as the average currents are zero in both cases. Consequently, additional indexes are required to detect this type of fault, which in turn requires extra calculations. A similar approach is presented in [22] for synchronous reluctance motors, where the average values of the powers are employed, along with adaptive thresholds that are automatically adjusted based on the operating conditions of the drive. In [23] a strategy based on normalized currents and zero-crossing detection is proposed to minimize distortions in current signals, ensuring the isolation of faulty switches even under transient load and frequency conditions. According to the proposed fault signals, only single or crossed switches OC faults can be detected and isolated. An OC FDI strategy for three-level NPC inverters is presented in [24]. The fault detection relies on the average current Park's vector, while the fault isolation is performed through post-processing of normalized currents divided into positive and negative half-cycles. Despite its demonstrated effectiveness under transient conditions, the fault detection stage has the drawback of exhibiting reduced sensitivity to full-leg faults, since it relies on the average current values. In addition, the fault-isolation algorithm requires several threshold comparisons and is not capable of diagnosing multiple OC faults.

In [25], a strategy based on the covariance analysis of IM three-phase currents is proposed to detect and isolate faults quickly and effectively. However, it can only diagnose single or full-leg OC faults. Moreover, in [26], a multiple OC FDI strategy based on normalizing the three-phase currents with a sliding window sampling is proposed. During the preprocessing stage, the frequency-domain features of the sampled signals are extracted using the principal components of the discrete Fourier transform. In [27], a fault feature extraction-based strategy is introduced, leveraging the duality of current-time pairs in closed-loop systems; however, it can only diagnose single OC faults. Due to the numerous stages involved in these diagnosis strategies, FDI entails a significant computational cost compared to other proposals.

Furthermore, in [28] a FDI strategy with a single current sensor for PMSM drives is proposed, based on the reconstruction of three-phase currents through a current measured on the DC-link, combined with zero-voltage vector sampling. This strategy enables to diagnosing single and double upper or lower OC faults. In addition, in [29] the single fault OC FDI is also performed through a single current sensor using a low-pass filter. This FDI does not need to reconstruct the three-phase currents because they are measured in the ED control. Unfortunately, these strategies cannot isolate all combinations of double-OC faults.

In the present work, a simple and effective signal-based FDI strategy is proposed for diagnosing both single and multiple OC faults in the inverter switches of an ED. The approach relies on zero-current interval analysis, where phase currents are decoupled into half-cycles. Then, the average values of the obtained signals are evaluated against a threshold value to generate diagnostic signals. Unlike [24], these signals are used for both detection and diagnosis, without requiring additional processing steps. In addition, a computationally efficient moving average calculation is proposed. This calculation simplifies FDI for a full-leg of the inverter and all other types of faults from the activation of the logic signals associated with the faulty switches. It should be highlighted that this strategy offers intrinsically faster detection, greater robustness against false alarms, and an easy-to-implement algorithm compared to those using the Park Vector transform [17] or the slope of trend lines [20]. Additionally, it requires tuning only a single threshold level, making its implementation relatively effortless.

Unlike [19], [20], [22]–[29] which can only isolate a subset of single or double OC faults, the present effort can detect and classify single, crossed, full-leg, two-upper or two-lower switch faults. Moreover, it does not require additional sensors, as in [21], [26], and it does not rely on the speed sensor to perform the FDI, as in [17], [21], [26], [29].

Table I summarizes the main characteristics of the related works together with the proposed FDI strategy. Although several strategies have been reported for detecting and isolating inverter switch faults, the proposed method offers the following advantages:

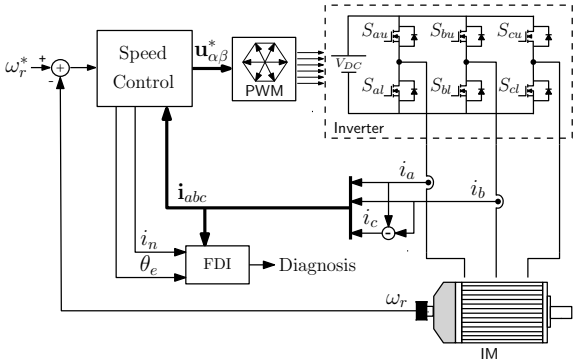

Fig. 1. General scheme of the IM drive and the FDI strategy.

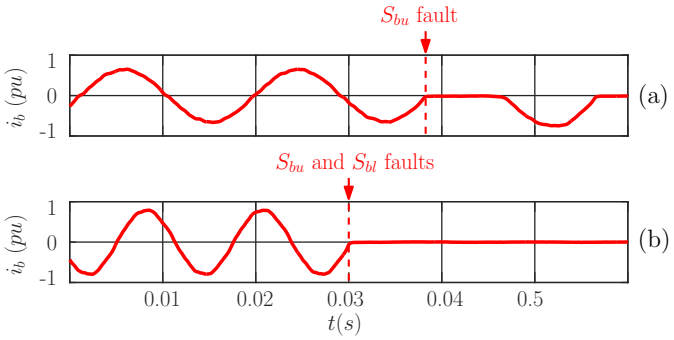

Fig. 2. Evolution of b phase current, i_b. (a) During a fault on S_{bu}. (b) During a fault on S_{bu} and S_{bl}.

- It does not require additional sensors or modification of the standard inverter topology.
- It is simple to implement in real time because it does not require complex mathematical computations.
- It is independent of the control strategy.
- It can detect and isolate single and multiple inverter open-switch faults.

Experimental validation using an IM drive shows that the FDI strategy can effectively perform the fault diagnosis under different motor operation conditions, considering different fault scenarios. Beyond its technical contribution, this work is particularly relevant to the Latin American context, where affordable and robust ED technologies are required. By enhancing the reliability and maintainability of ED systems through a simple and low-cost fault diagnostic strategy, it directly supports Sustainable Development Goal (SDG) 7 (Affordable and Clean Energy) and SDG 9 (Industry, Innovation and Infrastructure). Moreover, the computational efficiency and minimal hardware requirements of the proposed method enable scalable and sustainable embedded solutions in environments with limited technological resources, in line with SDG 12 (Responsible Consumption and Production).

The rest of the work is organized as follows. In Section II the fault detection and isolation strategy is described. Then, in Section III the experimental validation of the implemented diagnosis strategy is carried out.

II. Proposed Fault Detection and Isolation Strategy

The ED scheme shown in Fig. 1 is considered for the development of the proposed FDI strategy. Its scheme consists of a three-phase IM with a speed control strategy, an inverter, and sensors. The control inputs are the measurements of speed ω_r, and phase currents i_a and i_b. In addition, the current of phase c is obtained as $i_c = -i_a - i_b$. Based on this information and speed reference ω_r^*, the control strategy generates the voltage references fed to a PWM, $\mathbf{u}^*_{\alpha\beta}$. It is also considered that the control strategy generate a normalizing current i_n, and the electrical angle θ_e.

The inverter is composed of six semiconductor switches and their respective anti-parallel diodes. Each switch is denoted by S_{jk}, where $j \in \{a, b, c\}$ represents the corresponding phase, and $k \in \{u, l\}$ represents the upper or lower switch,

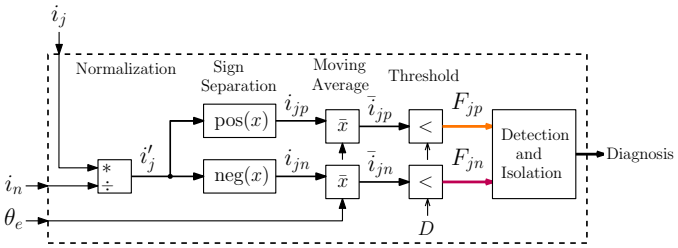

Fig. 3. Block diagram of the proposed inverter switch FDI strategy.

respectively. When an OC fault occurs in one of the inverter switches, the current flows only in a positive or negative direction during a part of the cycle, and is limited to zero for the rest of the cycle. This behavior is illustrated in the current patterns i_b shown in Fig. 2, obtained from experimental results. During a fault in the upper switch S_{bu}, the positive half cycle of the phase current b is equal to zero (see Fig. 2(a)); while if the fault occurs in a full leg, for example in S_{bu} and S_{bl}, the phase current is equal to zero (see Fig. 2(b)).

The diagram of the proposed strategy is shown in Fig. 3. The inputs are the phase currents i_j, the normalization current i_n, and the electrical angle θ_e. The output is the diagnosis, based on the state of the three logic signals F_{jp} and the three logic signals F_{jn}, associated with the fault in the upper and lower switches, respectively. The signal processing stages of the proposed strategy are described in the following.

A. Zero-current Interval Analysis

Since the amplitudes of the currents depend on the load coupled to the IM, torque variations have an impact on the current levels. To avoid this effect, the three-phase IM currents are normalized as:

$$i'_j = \frac{i_j}{i_n} \tag{1}$$

where i'_j represents the normalized currents. In addition, the value of i_n is obtained from the reference signals corresponding to the speed control.

TABLE I
COMPARISON OF THE PROPOSED FDI AND THOSE DEVELOPED IN THE LITERATURE

Article	Current Sensors	Speed Sensor	Single	Crossed	Full Leg	Two Upper or Lower
[17]	2	1	Yes	Yes	Yes	Yes
[18]	2	0	Yes	Yes	Yes	Yes
[19]	3	0	Yes	Yes	No	Yes
[20]	3	0	Yes	Yes	No	Yes
[21]	3	1	Yes	Yes	Yes	Yes
[22]	3	0	Yes	Yes	Yes	No
[23]	3	0	Yes	Yes	No	No
[24]	2	0	Yes	No	No	No
[25]	3	0	Yes	No	Yes	No
[26]	3	1	Yes	Yes	Yes	No
[27]	3	0	Yes	No	No	No
[28]	1	0	Yes	No	No	Yes
[29]	1	1	Yes	No	No	No
Proposed FDI	2	0	Yes	Yes	Yes	Yes

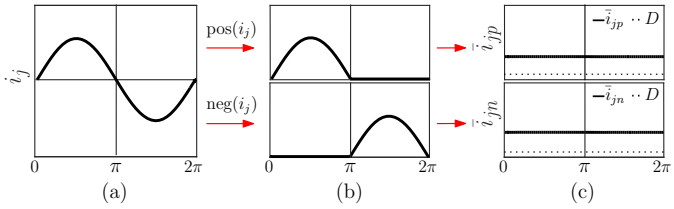

Fig. 4. Stages of calculation of the FDI strategy during the operation without fault. (a) Complete cycle. (b) Positive and negative separation. (c) Positive and negative average values.

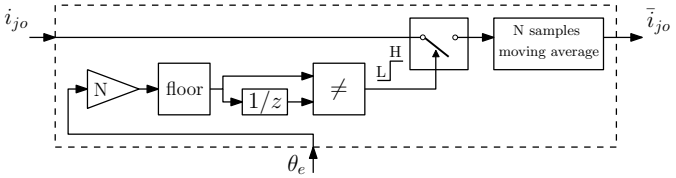

Fig. 5. Implementation of the moving average filter using a variable sampling clock based on the electrical angle.

The normalized currents are separated into positive (i_{jp}) and negative (i_{jn}) half-cycles as follows:

$$i_{jp} = \text{pos}(i'_j) = \begin{cases} i'_j & \text{if } i'_j > 0 \\ 0 & \text{if } i'_j \leq 0 \end{cases} \tag{2}$$

$$i_{jn} = \text{neg}(i'_j) = \begin{cases} |i'_j| & \text{if } i'_j < 0 \\ 0 & \text{if } i'_j \geq 0. \end{cases} \tag{3}$$

In this way, phase currents are decoupled as two signals sensitive to faults in the upper and lower switch of a leg; see Fig. 4.

B. Moving Average

In this stage, the signals obtained during normalization are averaged over a period using a moving average filter. In variable-speed ED, the electrical frequency depends on the operating point of the motor. Therefore, if a constant sampling time, it becomes necessary to dynamically adjust the number of integrated samples to compute the moving average, which requires a variable-sized buffer that is not straightforward to implement in real-time.

The implementation of the variable sampling time is based on the scheme shown in Fig. 5. The sampling clock is generated from the normalized angle θ_e, which varies between 0 and 1. Based on this signal, the floor function gives as output the greatest integer less than or equal to $N\theta_e$, where N represents the number of samples to be averaged. This constant number is $N <= f_s/f_n$, where f_s represents the sample frequency and f_n the rated frequency, respectively. Subsequently, changes in the integer values of the electrical angle are detected to generate the sampling clock.

The moving average value is calculated for the separated phase currents i_{jo}, where the subscript $o \in \{p, n\}$. By using the proposed variable frequency sampling clock, the number of samples N remains constant, which allows the implementation of a simple moving average, defined as:

$$\bar{i}_{jo}[k] = \bar{i}_{jo}[k-1] + \frac{1}{N}\left(i_{jo}[k] - i_{jo}[k-N]\right) \tag{4}$$

where $\bar{i}_{jo}$ is the obtained current average value. Note that (4) requires only three arithmetic operations and a circular buffer.

C. Fault Detection

During normal operation, the average values of the currents $\bar{i}_{jo}$ (4) remain above a threshold level, while when a fault occurs on the inverter switches, they acquire a value close to zero. Therefore, in order to detect the OC fault, a fixed threshold is used. If one or more of the signals $\bar{i}_{jo}$ decrease below the threshold level, a fault is reported. Fault signals are described as follows

$$F_{jo} = \begin{cases} 0 & \text{if } |\bar{i}_{jo}| \geq D, \\ 1 & \text{if } |\bar{i}_{jo}| < D. \end{cases} \tag{5}$$

Assuming a faultless operation and perfect normalization, $\bar{i}_{jo}$ will have a value of 0.3183. The threshold level was defined as D = 0.03183, corresponding to 10% of $\bar{i}_{jo}$ under the rated condition, see Fig. 4. It should be noted that increasing the threshold can enable earlier fault detection, but it also increases the likelihood of false positives due to sudden torque or speed variations. Consequently, the selected threshold provides an appropriate balance between detection speed (approximately

TABLE II
RELATIONSHIP BETWEEN THE FAULT SIGNALS AND THE CORRESPONDING DIAGNOSIS FOR EACH INVERTER OC FAULT TYPE

F_{ap}	F_{an}	F_{bp}	F_{bn}	F_{cp}	F_{cn}	Case	**Diagnosis**
0	0	0	0	0	0	-	HEALTHY
1	0	1	0	0	1	3	S_{au} S_{bu}
1	0	0	1	1	0	3	S_{au} S_{cu}
0	1	1	0	1	0	3	S_{bu} S_{cu}
0	1	0	1	1	0	3	S_{al} S_{bl}
0	1	1	0	0	1	3	S_{al} S_{cl}
1	0	0	1	0	1	3	S_{bl} S_{cl}
1	0	0	1	0	0	2	S_{au} S_{bl}
1	0	0	0	0	1	2	S_{au} S_{cl}
0	1	1	0	0	0	2	S_{al} S_{bu}
0	0	1	0	0	1	2	S_{bu} S_{cl}
0	1	0	0	1	0	2	S_{al} S_{cu}
0	0	1	0	0	1	2	S_{bl} S_{cu}
1	1	0	0	0	0	2	S_{au} S_{al}
0	0	1	1	0	0	2	S_{bu} S_{bl}
0	0	0	0	1	1	2	S_{cu} S_{cl}
1	0	0	0	0	0	1	S_{au}
0	1	0	0	0	0	1	S_{al}
0	0	1	0	0	0	1	S_{bu}
0	0	0	1	0	0	1	S_{bl}
0	0	0	0	1	0	1	S_{cu}
0	0	0	0	0	1	1	S_{cl}

one electrical cycle) and robustness for OC faults in the inverter switches. The activation of any of the fault signals indicates the detection of a fault.

The following section describes the isolation processing performed in case that a fault is detected.

D. Fault Isolation

The isolation process starts after the fault is detected. This process involves analyzing the activation of the fault signals F_{jo}, according to the flow chart in Fig. 6. As shown in this figure, the activation of three fault signals indicates a fault in either two upper or two lower switches, which is classified as Case 3. It is worth mentioning that the third fault signal is activated because $i_c = -i_a - i_b$.

If two fault signals are activated, this indicates either a full leg open circuit (OC) or a cross fault OC, which corresponds to Case 2. When only one fault signal is activated, it is classified as Case 1, indicating a fault in a single switch.

The final fault isolation is performed according to Table II, which details the diagnosis for all fault cases. It is worth mentioning that after the diagnosis is performed, if a new fault signal is activated, a new isolation cycle is started.

III. EXPERIMENTAL VALIDATION

The experimental setup used to test the proposed FDI strategy is shown in Fig. 7. It consists of a 0.75 kW IM, with its rated variables are listed in Table III, coupled to a load machine controlled by an industrial controller. The IM is powered by an inverter connected to the electrical grid via a rectifier. A field-oriented control (FOC) and the proposed FDI strategies were implemented in a Texas Instruments

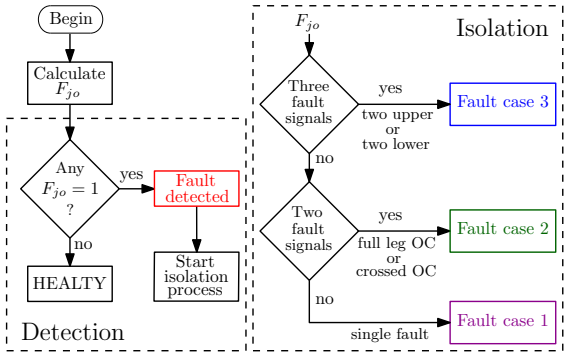

Fig. 6. Flowchart of the FDI algorithm for identifying single and multiple OC faults.

TABLE III
INDUCTION MOTOR AND DIAGNOSING PARAMETERS

Power	0.75 kW		
Rated frequency f_n	50 Hz		
Line voltage (RMS)	26.4 V		
Phase current (RMS)	32.3 A		
Rated speed	1435 RPM		
R_s	69.7 mΩ	R_r	34.71 mΩ
L_s, L_r	0.11 mH	L_m	2.66 mH
P	2	J	0.002 94 kg m^2
Sample frequency f_s	10 kHz		
Number of samples N	21		
DC-link voltage V_{DC}	42 V		

TMS320F28335 DSP. The FOC (see Fig. 8) takes as inputs the stator currents $\mathbf{i}_{abc}$ and the rotor speed ω_r, to compute the reference voltages $\mathbf{u}^*_{\alpha\beta} = \left[u^*_\alpha, u^*_\beta\right]^T$, which are fed to a PWM with a switching frequency of 10 kHz. Internally, the FOC generates the signal θ_e, representing the phase angle of the inverter voltages, and the normalization current, obtained as $i_n = \text{mod}(i^*_q, i^*_d) = \sqrt{(i^*_d)^2 + (i^*_q)^2}$ (see Fig. 1) where i^*_d and i^*_q are the reference currents. Additionally, a computer and a debug interface were used to set reference values, acquire data and deactivate switching signals to emulate the OC faults.

Based on the described experimental setup, two different sets of tests were performed: the first set verified the FDI under different operating points of the IM; and in the second set, the effectiveness of the strategy to diagnose different types of faults was verified. It is worth mentioning that, in healthy condition tests, data were acquired with a sampling period of 2 kSPS, while in fault condition tests, data were acquired at 10 kSPS, with a total of 1300 samples.

A. FDI Performance during Healthy Condition

A test was performed to analyze the performance of the FDI strategy against a sudden variation in the load torque, and the results obtained are shown in Fig. 9. At t = 0 s, the IM speed is 0.5 pu and the load torque is 0.3 pu. Then, at t = 0.1 s, the load torque is increased to 0.7 pu. As can be seen in Fig. 9(a), the load variation produces a temporary decrease of ω_r until t = 0.3 s, when it reaches the reference value. Furthermore, currents peak values increase as a result of the load torque, see Fig. 9(b). On the other hand, throughout the test, the average

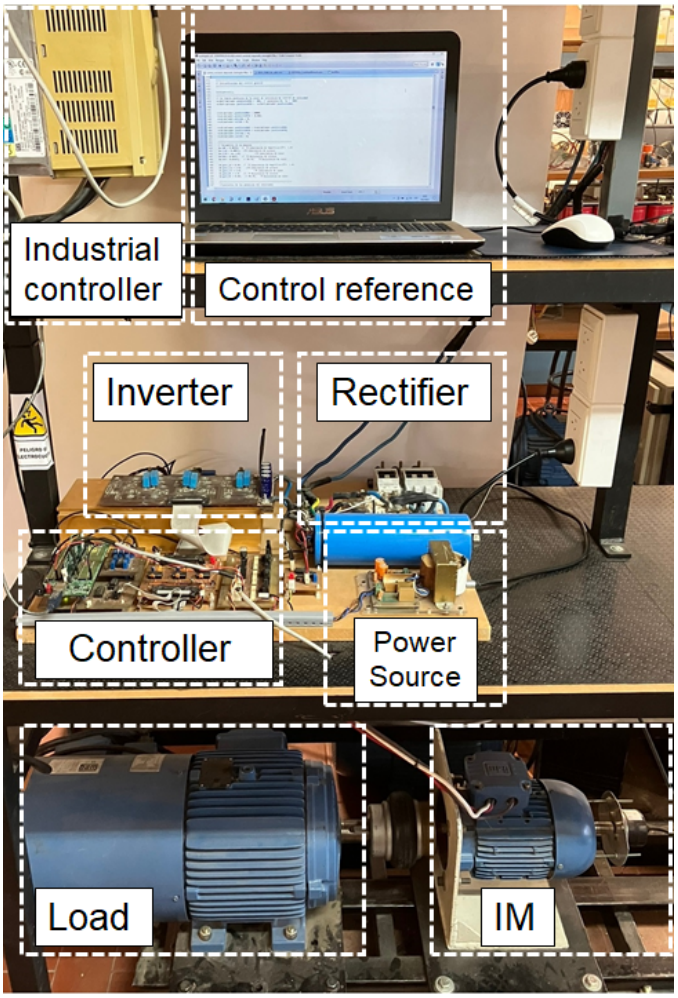

Fig. 7. Experimental setup used to validate the proposed FDI strategy.

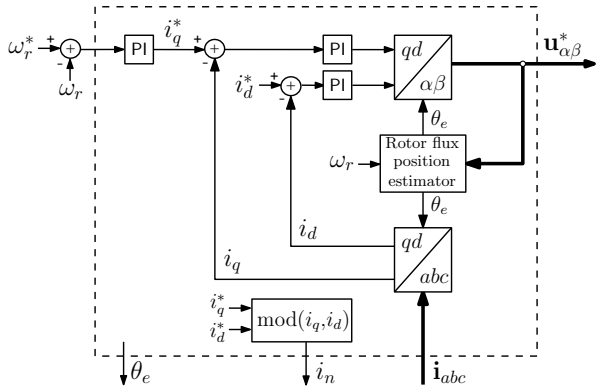

Fig. 8. Structure of the FOC speed controller and generation of the variables used by the FDI strategy.

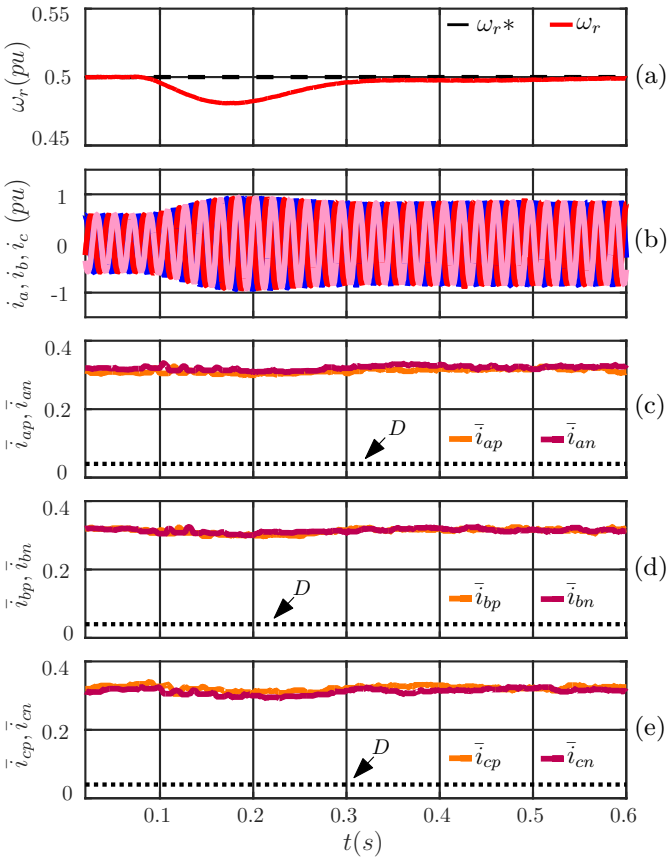

Fig. 9. Performance under torque step. (a) Rotor speed, ω_r. (b) Phase currents i_a, i_b, i_c. (c) Average value of the positive and negative separation of a. (d) Average value of the positive and negative separation of b. (e) Average value of the positive and negative separation of c.

values corresponding to the positive and negative separation (see Fig. 3) of the phase currents a, b and c shown in Fig. 9(c), (d) and (e), respectively, remain over the threshold value D.

In addition, a speed variation test was also performed. The obtained results are shown in Fig. 10 where the IM is operating at a speed of 0.3 pu and the load torque is 0.5 pu at t = 0 s. During the time interval 0.1 s < t < 0.5 s, the speed is increased to 0.7 pu. Then, the current peak values increases to 1.15 pu as shown in Fig. 10(b). Furthermore, the average values shown in Fig. 10(c), (d) and (e) remain over the threshold level D throughout the test.

From the results shown in Fig. 9 and Fig. 10, it can be concluded that the proposed average values remain above the threshold level D during variations in speed and load torque.

B. FDI Performance under OC Switch Faults

When an inverter switch fails, the FOC attempts to maintain the torque and reference flux. As a result, the amplitude of the phase currents increases, and due to the loss of the affected half-cycle, oscillations occur in the motor torque along with a reduction of its average value. This is reflected in a decrease in the rotor speed. Based on these observations, the following fault tests were performed to analyze the performance of the FDI strategy:

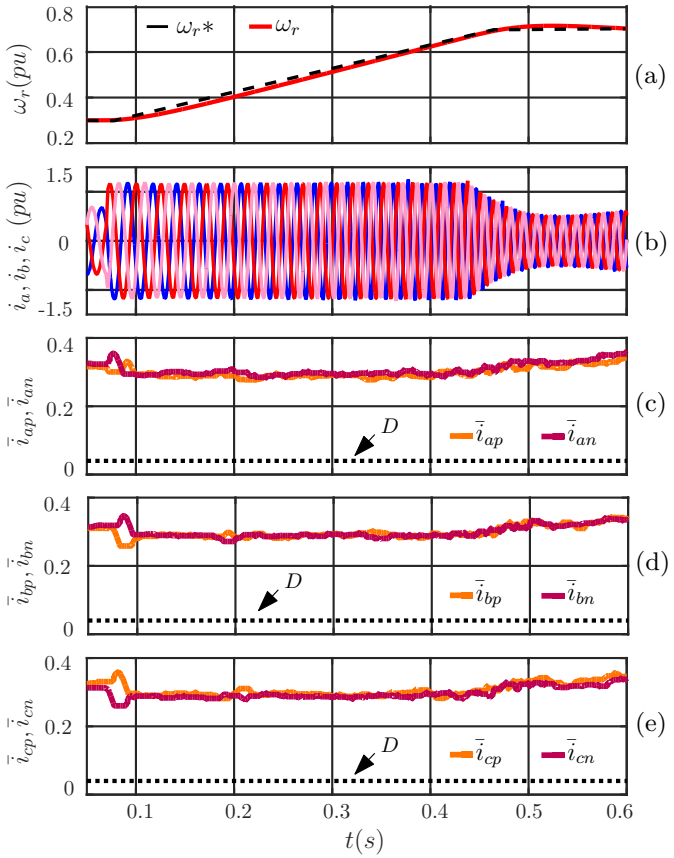

Fig. 10. Performance under speed ramp. (a) Rotor speed, ω_r. (b) Phase currents i_a, i_b, i_c. (c) Average value of the positive and negative separation of a. (d) Average value of the positive and negative separation of b. (e) Average value of the positive and negative separation of c.

- Fault in full leg b (S_{bu} and S_{bl}).
- Faults in cross switches (S_{bu} and S_{cl}).
- Faults in two upper switches (S_{bu} and S_{au}).

The results shown in Fig. 11 were performed with the IM operating at a speed of 0.75 pu and a load torque of 0.7 pu. Fig. 11(a) shows the rotor speed ω_r and the speed reference ω_r^*, while Fig. 11(b) shows phase currents i_a, i_b, and i_c. At t = 0.03 s simultaneous faults occur in switches S_{bu} and S_{bl}, therefore the value of the phase current b becomes equal to zero. Fig. 11(c) shows the average values corresponding to the positive and negative separation of i_b. After the fault of S_{bu}, $\bar{i}_{bp}$ decreases until it reaches a value below the threshold D and produces the activation of F_{bp}, indicating the fault detection. Furthermore, at t = 0.037 s the signal $\bar{i}_{bn}$ decreases below D and F_{bn} is activated, indicating another fault. Referring to the FDI algorithm described in Fig. 6 the activation of two fault signals corresponds to the fault case 2, and, according to Table II, it indicates a full leg fault (S_{bu}, S_{bl}). It is worth mentioning that the FDI of the full leg fault is carried out at t = 0.044 s, approximately one electrical cycle after the fault occurs for the analyzed operating point.

The results shown in Fig. 12 were performed with the IM operating at a speed of 0.5 pu with a load torque of 0.5 pu. OC faults occurs in S_{bu} and S_{cl} at t = 0.038 s and

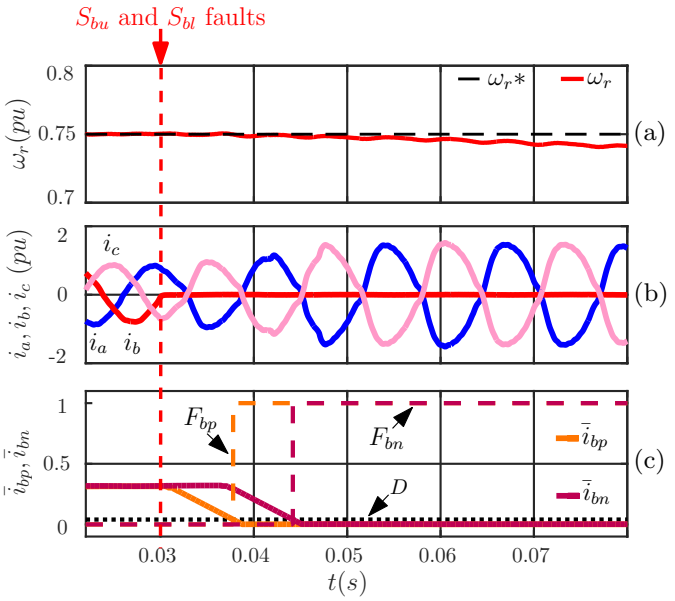

Fig. 11. Fault in S_{bu} and S_{bl} of the inverter. (a) Rotor speed, ω_r. (b) Phase currents i_a, i_b, i_c. (c) Average value of the positive and negative separation of b, and fault signals F_{bp}, F_{bn}.

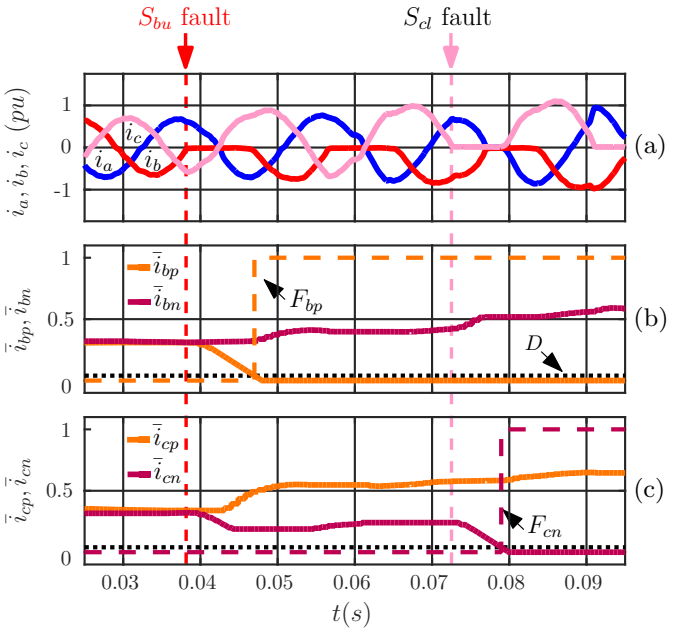

Fig. 12. Faults in switches S_{bu} and S_{cl}. (a) Phase currents i_a, i_b, i_c. (b) Average value of the positive and negative separation of b, and fault signal F_{bp}. (c) Average value of the positive and negative separation of c, and fault signal F_{cn}.

t = 0.073 s, respectively. Furthermore, in Fig. 12(a) it can be seen that after the fault at S_{bu}, the signal $\bar{i}_{bp}$ decreases below D and triggering the fault signal F_{bp} at t = 0.047 s, which activates the detection and isolates the faulty switch, as shown in Fig. 12(b). Also, the second fault is isolated at t = 0.079 s, see Fig. 12(c). For the analyzed operating point, the isolation after of each fault is carried out within half an electrical cycle; see Fig. 12(a).

The results shown in Fig. 13 were performed with the IM

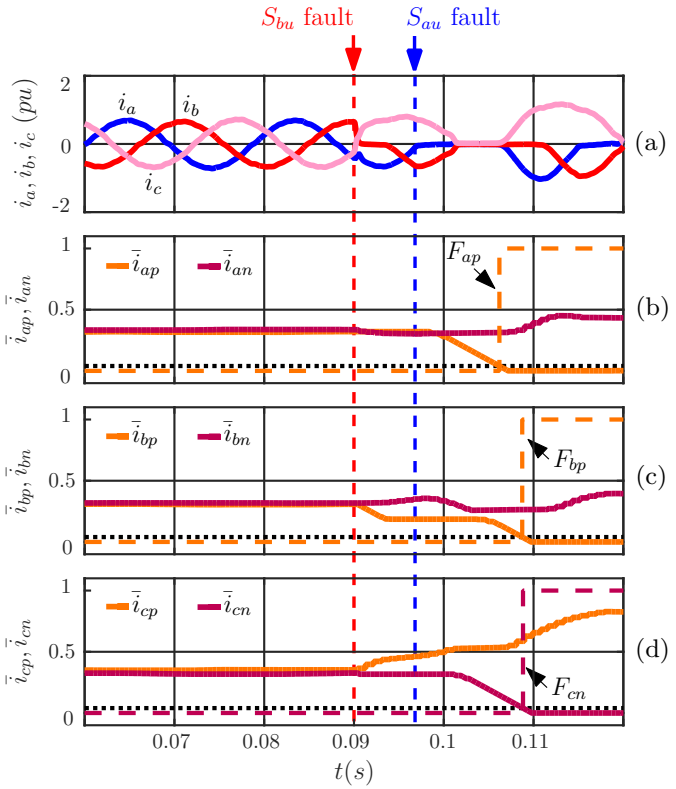

Fig. 13. Faults in switches S_{bu} and S_{au}. (a) Phase currents i_a, i_b, i_c. (b) Average value of the positive and negative separation of a, and fault signal F_{ap}. (c) Average value of the positive and negative separation of b, and fault signal F_{bp}. (d) Average value of the positive and negative separation of c, and fault signal F_{cn}.

operating at a speed of 0.5 pu and a load torque of 0.5 pu. The OC faults occurs in S_{bu} and S_{au} at t = 0.09 s and t = 0.097 s, respectively, as shown in Fig. 13(a). After the fault in S_{bu} and S_{au} it can be seen in Figs. 13(b) and (c) that the signals $\bar{i}_{ap}$ and $\bar{i}_{bp}$ decrease below the threshold and activate the fault signals F_{ap} at t = 0.0106 s and F_{bp} at t = 0.0108 s, respectively. Furthermore, $\bar{i}_{cn}$ also decreases below D and produces the activation of F_{cn} at t = 0.0108 s, see Fig. 13(d). Once F_{ap} is activated, fault detection is performed, and the S_{au} switch is isolated within half an electrical cycle after the fault. Subsequently, based on the fault signals F_{bp} and F_{cn}, the second faulty switch is isolated within one electrical cycle after the fault occurrence. The three triggered fault signals (F_{ap}, F_{bp}, and F_{cn}) determine a fault case 3 (two upper fault), being S_{au} and S_{bu} the affected switches according to Table II.

The results show that the FDI strategy for inverter switches identifies single, crossed, full leg, and two upper or lower OC faults in less than one electrical cycle after the occurrence of each fault.

C. Comparison with other Proposals

Based on the reviewed literature and the characteristics summarized in Table I, it can be observed that some works, such as [17], [18], [21], are capable of diagnosing all combinations of single and double OC inverter faults. In particular, in [18] the signal-based FDI strategy combines ease of implementation with low computational cost, while enabling the detection of both single and multiple faults. This work was therefore taken as a reference to evaluate the proposed strategy against existing approaches in the literature. In the reference work, the FDI strategy is based on the analysis of the fault indexes δ_j, with $j \in \{a, b, c\}$, and P_N, defined as:

$$\delta_j[k] = \frac{\bar{i}'_j[k]}{\rho + |\bar{i}'_j[k]|} \tag{6}$$

$$P_N[k] = \frac{i_\alpha[k] - i_\alpha[k-1]}{i_\beta[k] - i_\beta[k-1]} \tag{7}$$

where the constant $\rho = \frac{\sqrt{8}}{\pi\sqrt{3}}$, $[i_\alpha, i_\beta]$ are the phase currents in the α-β frame after the Clarke transformation and the overline represents the mean value. Note that in this proposal the currents are also sampled using a constant number of samples N per fundamental period.

The fault is detected when the signal P_N remains within one of the three predefined bands during M consecutive samples. Depending on the band in which P_N is detected, one of the three fault detection signals F_{Pj} is activated, corresponding to the following criteria:

$$F_{Pa} = \begin{cases} 1, & \text{if } \left|P_N[n] - P_{th}\right| < 0, \quad \forall n \in [k-M,\, k] \\ 0, & \text{otherwise} \end{cases}$$

$$F_{Pb} = \begin{cases} 1, & \text{if } \left|P_N[n] - P_{th}\right| < \sqrt{3}, \quad \forall n \in [k-M,\, k] \\ 0, & \text{otherwise} \end{cases}$$

$$F_{Pc} = \begin{cases} 1, & \text{if } \left|P_N[n] - P_{th}\right| < -\sqrt{3}, \quad \forall n \in [k-M,\, k] \\ 0, & \text{otherwise} \end{cases} \tag{8}$$

where P_{th} is a constant threshold. The fault isolation is carried out after the activation of any F_{Pj} signal, when the corresponding δ_j exceeds the threshold δ_{th} or falls below $-\delta_{th}$.

One of the main disadvantages of this strategy is that it relies on the first-order difference operation, which can make it sensitive to noise in current measurements. In order to analyze this sensitivity, new results were obtained using the reference strategy and the proposed FDI. The results shown in Figs. 14 and 15 were obtained during a no-load test at rated frequency. A no-load test was selected, since it exhibited higher current noise levels compared to the current magnitude observed in the experiments. Two consecutive OC faults occur during these tests, in S_{au} and S_{bl} at t = 0.06 s and t = 0.1 s, respectively. The results shown in Fig. 14 were obtained using the parameters $P_{th} = 0.2$ and $M = 5$, as proposed in [18], and $N = 21$. As shown in Fig. 14(a), after the fault in S_{au}, the positive half-cycle of i_a drops to zero, and P_N remains inside the central band for M successive samples at $t = 0.088$ s (see Fig. 14(b)), which triggers the F_{Pa} fault signal. Note that the first rectified half-cycle was not detected. Subsequently, at $t = 0.1$ s, the S_{bl} fault occurs, and as shown in Fig. 14(a), the negative half-cycle of i_b drops to zero. However, as shown in Fig. 14(b), the number of samples required inside the upper band to activate the F_{Pb} fault signal is insufficient to trigger the second fault detection, see Fig. 14(c).

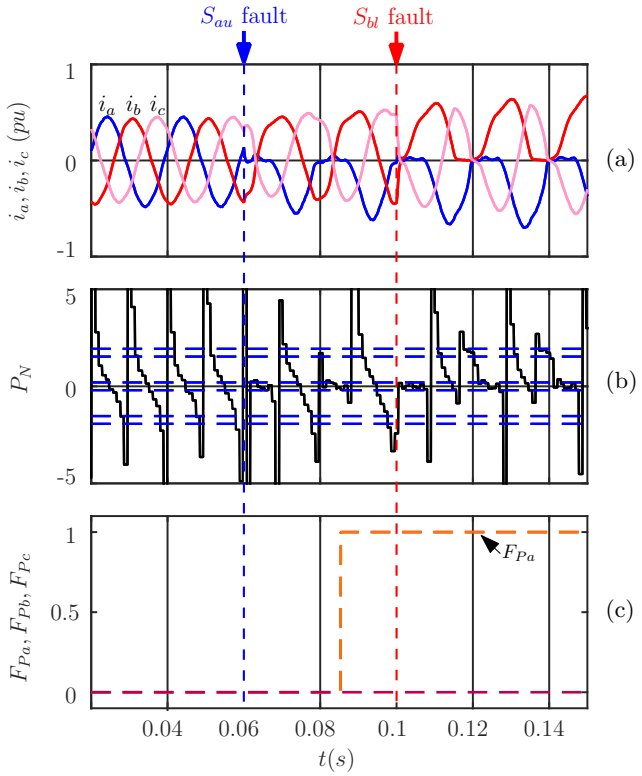

Fig. 14. Faults in switches S_{au} and S_{bl} with parameters proposed in [18]. (a) Phase currents i_a, i_b, i_c. (b) Detection signal P_N. (c) Fault signals F_{Pa}, F_{Pb} and F_{Pc} from reference FDI strategy.

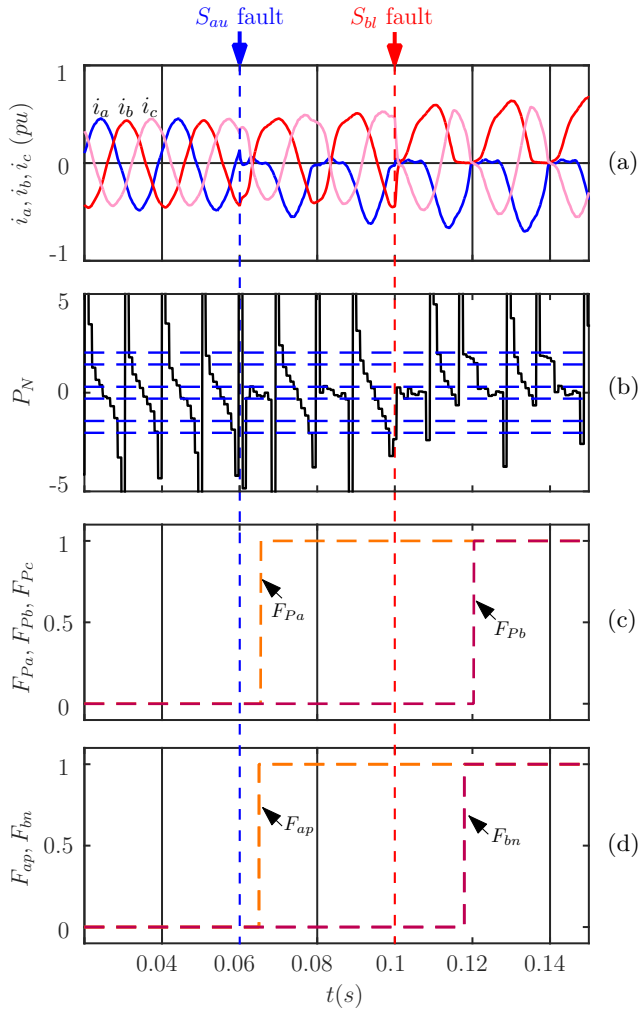

Fig. 15. Faults in switches S_{au} and S_{bl} with modified parameters and filtered currents. (a) Phase currents i_a, i_b, i_c. (b) Detection signal P_N. (c) Fault signals F_{Pa}, F_{Pb} and F_{Pc} from reference FDI strategy. (d) Proposed fault signals F_{ap} and F_{bn}.

The results shown in Fig. 15 were obtained after extensive parameter tuning to achieve a more accurate diagnosis, with $N = 21$. In this additional test, the measured currents were filtered using a digital low-pass filter with a cutoff frequency of 850 Hz in order to reduce the noise effect. Moreover, the parameters $P_{th} = 0.4$ and $M = 4$ were selected. Based on these values, it can be seen in Fig. 15(b) that P_N signal properly remains in the middle and the upper bands after each fault, triggering the associated fault signals, see Fig. 15(c). In addition, Fig. 15(d) shows the fault signals of the FDI strategy proposed in this work without the low-pass filter, where it can be observed that the FDI exhibits a slightly faster response time than the previous diagnosis, without requiring the adjustment of any additional parameters. Specifically, the first fault is detected at 6 ms with the proposed strategy and at 6.4 ms with the reference strategy; the second fault is detected at 17.9 ms and 20.3 ms, respectively.

The obtained results show that the FDI strategy proposed in [18] can effectively detect consecutive faults, but it requires more effort in parameter adjustments. For a more comprehensive comparison with existing approaches, the Table IV summarizes the number of logic fault detection signal to be generated and the number of parameters to be tuned for some simple FDI strategies reported in the literature. The comparison shows that the strategy proposed in this work requires fewer parameter tunings and fewer indices to be analyzed.

TABLE IV
FAULT DIAGNOSTIC METHODS KEY FEATURES EVALUATION

Article	Fault detection signals	Parameters to tune
[17]	7	4
[18]	4	3
[21]	6	3
Proposed FDI	6	1

IV. CONCLUSION

In this work, a new fault detection and isolation (FDI) strategy was presented for diagnosing single and multiple inverter open-switch faults in an electric drive, based on zero current interval analysis. The proposed FDI strategy does not require additional hardware or complex mathematical computations. To demonstrate the performance of the FDI strategy, an electric drive with field oriented control (FOC) was used to vary the operating point of an induction motor. Furthermore, different tests were performed under simultaneous and consecutive OC faults such as crossed, full leg, and two upper to evaluate the

effectiveness of the diagnosis.

Experimental results demonstrate that the proposed FDI strategy does not generate false positives when speed and torque variations occur during normal operation. In addition, the strategy allows detecting and isolating single and multiple faults in the inverter switches. Moreover, the proposed FDI strategy achieves effective consecutive fault detection with faster response and fewer parameters and indices to analyze compared to the reference method, demonstrating a more efficient and robust fault diagnosis approach.

REFERENCES

[1] S. Yang, A. Bryant, P. Mawby, D. Xiang, L. Ran, and P. Tavner, "An industry-based survey of reliability in power electronic converters," *IEEE Transactions on Industry Applications*, vol. 47, no. 3, pp. 1441–1451, 2011. doi: 10.1109/TIA.2011.2124436 .

[2] Y. Wu, G. F. Olson, C. Henriksson, and L. Peretti, "Open fault detection in variable phase-pole machines based on harmonic plane decomposition," *IEEE Transactions on Power Electronics*, vol. 39, no. 4, pp. 4557–4566, 2024. doi: 10.1109/TPEL.2023.3348973 .

[3] K. Hu, Z. Liu, Y. Yang, F. Iannuzzo, and F. Blaabjerg, "Ensuring a reliable operation of two-level IGBT-based power converters: A review of monitoring and fault-tolerant approaches," *IEEE Access*, vol. 8, pp. 89 988–90 022, 2020. doi: 10.1109/ACCESS.2020.2994368 .

[4] M. Alavi, D. Wang, and M. Luo, "Short-Circuit Fault Diagnosis for Three-Phase Inverters Based on Voltage-Space Patterns," *IEEE Transactions on Industrial Electronics*, vol. 61, no. 10, pp. 5558–5569, 2014. doi: 10.1109/TIE.2013.2297298 .

[5] U.-M. Choi, F. Blaabjerg, and K.-B. Lee, "Study and handling methods of power IGBT module failures in power electronic converter systems," *IEEE Transactions on Power Electronics*, vol. 30, no. 5, pp. 2517–2533, 2015. doi: 10.1109/TPEL.2014.2373390 .

[6] Z. Gao, S. X. Ding, and C. Cecati, "Real-time fault diagnosis and fault-tolerant control," *IEEE Transactions on industrial Electronics*, vol. 62, no. 6, pp. 3752–3756, 2015. doi: 10.1109/TIE.2015.2417511 .

[7] C. Yong, J.-j. Zhang, and Z.-y. Chen, "Current observer-based online open-switch fault diagnosis for voltage-source inverter," *ISA transactions*, vol. 99, pp. 445–453, 2020. doi: 10.1016/j.isatra.2019.09.019 .

[8] S. Xu, X. Chen, F. Liu, H. Wang, Y. Chai, W. X. Zheng, and H. Chen, "A Novel Adaptive SMO-Based Simultaneous Diagnosis Method for IGBT Open-Circuit Faults and Current Sensor Incipient Faults of Inverters in PMSM Drives for Electric Vehicles," *IEEE Transactions on Instrumentation and Measurement*, vol. 72, pp. 1–15, 2023. doi: 10.1109/TIM.2023.3305653 .

[9] F. Naseri, E. Schaltz, K. Lu, and E. Farjah, "Real-time open-switch fault diagnosis in automotive permanent magnet synchronous motor drives based on kalman filter," *IET Power Electronics*, vol. 13, no. 12, pp. 2450–2460, 2020. doi: 10.1049/iet-pel.2019.1498 .

[10] H. Yan, Y. Xu, F. Cai, H. Zhang, W. Zhao, and C. Gerada, "PWM-VSI fault diagnosis for a PMSM drive based on the fuzzy logic approach," *IEEE Transactions on Power Electronics*, vol. 34, no. 1, pp. 759–768, 2019. doi: 10.1109/TPEL.2018.2814615 .

[11] C. N. Ibem, M. E. Farrag, A. A. Aboushady, and S. M. Dabour, "Multiple open switch fault diagnosis of three phase voltage source inverter using ensemble bagged tree machine learning technique," *IEEE Access*, 2023. doi: 10.1109/ACCESS.2023.3304238 .

[12] I. Bandyopadhyay, P. Purkait, and C. Koley, "Performance of a classifier based on time-domain features for incipient fault detection in inverter drives," *IEEE Transactions on Industrial Informatics*, vol. 15, no. 1, pp. 3–14, 2019. doi: 10.1109/TII.2018.2854885 .

[13] H. Yan, Y. Peng, W. Shang, and D. Kong, "Open-circuit fault diagnosis in voltage source inverter for motor drive by using deep neural network," *Engineering Applications of Artificial Intelligence*, vol. 120, p. 105866, 2023. doi: 10.1016/j.engappai.2023.105866 .

[14] C. Choi and W. Lee, "Design and evaluation of voltage measurement-based sectoral diagnosis method for inverter open switch faults of permanent magnet synchronous motor drives," *IET Electric Power Applications*, vol. 6, no. 8, pp. 526–532, 2012. doi: 10.1049/iet-epa.2011.0315 .

[15] Z. Li, H. Ma, Z. Bai, Y. Wang, and B. Wang, "Fast transistor open-circuit faults diagnosis in grid-tied three-phase VSIs based on average bridge arm pole-to-pole voltages and error-adaptive thresholds," *IEEE Transactions on Power Electronics*, vol. 33, no. 9, pp. 8040–8051, 2017. doi: 10.1109/TPEL.2017.2773130 .

[16] M. A. Rodríguez-Blanco, A. Vazquez-Perez, L. Hernandez-Gonzalez, V. Golikov, J. Aguayo-Alquicira, and M. May-Alarcon, "Fault detection for IGBT using adaptive thresholds during the turn-on transient," *IEEE Transactions on Industrial Electronics*, vol. 62, no. 3, pp. 1975–1983, 2014. doi: 10.1109/TIE.2014.2364154 .

[17] C.-J. Bae, D.-C. Lee, and T. H. Nguyen, "Detection and identification of multiple IGBT open-circuit faults in PWM inverters for AC machine drives," *IET Power Electronics*, vol. 12, no. 4, pp. 923–931, 2019. doi: 10.1049/iet-pel.2018.5188 .

[18] M. Trabelsi, M. Boussak, and M. Benbouzid, "Multiple criteria for high performance real-time diagnostic of single and multiple open-switch faults in ac-motor drives: Application to IGBT-based voltage source inverter," *Electric Power Systems Research*, vol. 144, pp. 136–149, 2017. doi: 10.1016/j.epsr.2016.11.021 .

[19] D. U. Campos-Delgado, J. A. Pecina-Sánchez, D. R. Espinoza-Trejo, and E. R. Arce-Santana, "Diagnosis of open-switch faults in variable speed drives by stator current analysis and pattern recognition," *IET Electric Power Applicat.*, vol. 7, no. 6, pp. 509–522, 2013. doi: 10.1049/iet-epa.2013.0015 .

[20] X. Sun, N. Diao, C. Song, Y. Qiu, and X. Zhao, "An Open-Circuit Fault Diagnosis Method Based on Adjacent Trend Line Relationship of Current Vector Trajectory for Motor Drive Inverter," *Machines*, vol. 11, no. 10, p. 928, 2023. doi: 10.3390/machines11100928 .

[21] I. Jlassi and A. J. M. Cardoso, "A Single Method for Multiple IGBTs, Current-and Speed-Sensor Faults Diagnosis in Regenerative PMSM Drives," *IEEE Trans. Emerg. Sel. Topics Power Electron.*, 2020. doi: 10.1109/JESTPE.2019.2918062 .

[22] M. Salman, J. Riccio, S. K. El Khil, P. Zanchetta, and C. Boccaletti, "Unified Diagnosis and Localization Method of Open Switch Faults in Voltage Source Inverters-Fed Synchronous Reluctance Motors," *IEEE Transactions on Industry Applications*, 2025. doi: 10.1109/TIA.2025.3577113 .

[23] Z. Jian-Jian, C. Yong, C. Zhang-Yong, and Z. Anjian, "Open-Switch Fault Diagnosis Method in Voltage-Source Inverters Based on Phase Currents," *IEEE Access*, vol. 7, pp. 63 619–63 625, 2019. doi: 10.1109/ACCESS.2019.2913164 .

[24] A. M. S. Mendes, M. B. Abadi, and S. M. A. Cruz, "Fault diagnostic algorithm for three-level neutral point clamped ac motor drives, based on the average current park's vector," *IET Power Electronics*, vol. 7, no. 5, pp. 1127–1137, 2014.

[25] H. Yang, Y. Zhou, and J. Zhao, "Current covariance analysis-based open-circuit fault diagnosis for voltage-source-inverter-fed vector-controlled induction motor drives," *Journal of Power Electronics*, vol. 20, pp. 492–500, 2020. doi: 10.1007/s43236-020-00043-5 .

[26] X. Sun, C. Song, Y. Zhang, X. Sha, and N. Diao, "An Open-Circuit Fault Diagnosis Algorithm Based on Signal Normalization Preprocessing for Motor Drive Inverter," *IEEE Transactions on Instrumentation and Measurement*, vol. 72, pp. 1–12, 2023. doi: 10.1109/TIM.2023.3268461 .

[27] C. Song, X. Zhao, X. Sun, N. Diao, and J. Zhao, "Fast in-loop single-tube open-circuit fault diagnosis for voltage source inverter based on duality of current-time pairs," *IEEE Transactions on Industrial Electronics*, vol. 70, no. 9, pp. 9572–9581, 2023. doi: 10.1109/TIE.2022.3212398 .

[28] H. Yan, Y. Xu, J. Zou, Y. Fang, and F. Cai, "A novel open-circuit fault diagnosis method for voltage source inverters with a single current sensor," *IEEE Transactions on Power Electronics*, vol. 33, no. 10, pp. 8775–8786, 2018. doi: 10.1109/TPEL.2017.2776939 .

[29] Z. Chen, D. Liang, S. Jia, S. Yang, and L. Yang, "A simple open-switch fault detection and diagnosis method for permanent magnet synchronous machines drive system based on DC-link current," *IET Power Electronics*, vol. 16, no. 4, pp. 584–595, 2022. doi: 10.1049/pel2.12410 .

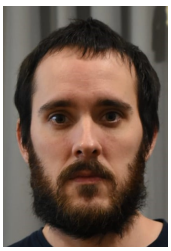

Luis E. Venghi received his degree in Electronic Engineering in 2016, from Universidad Nacional de San Luis, San Luis, Argentina. He also received his PhD degree in Engineering Sciences in 2022, at the National University of Río Cuarto, Córdoba, Argentina. He is currently a Postdoctoral Fellow of CONICET and member of the Research and Transfer Center of the National University of Rafaela, Santa Fe, Argentina. His topics of interest are: electric drives, fault diagnosis, fault tolerance and electric vehicles.

Facundo Aguilera (S'05 - M'14 - SM'20) received his degree in Electronic Engineering with Orientation in Digital Systems from the Universidad Nacional de San Luis, in 2009, and the Doctorate Degree in Engineering Science from the Universidad Nacional de Río Cuarto (UNRC), Argentina, in 2015. In 2010, he joined the Grupo de Electrónica Aplicada (GEA), UNRC. He is currently professor with the UNRC and Asistant Researcher with the Consejo Nacional de Investigaciones Científicas y Técnicas (CONICET), Argentina. He is currently president of the IEEE Joint Chapter#1 (IE13/CS23/RA24/IA34/PEL35/VT06), Argentina Section. His research interests include electric vehicles traction, fault tolerant power electric converters and renewable-energy generation.

Pablo M. de la Barrera (Senior Member, IEEE) received his B.Sc. and M.Sc. degrees in electrical engineering from the Universidad Nacional de Río Cuarto, Río Cuarto, in 2003 and 2006, respectively, and the Ph.D. degree in control systems from the Universidad Nacional del Sur, Bahía Blanca, Argentina, in 2009. Since 1998, he has been with the Grupo de Electrónica Aplicada, Universidad Nacional de Río Cuarto. He is also with the Consejo Nacional de Investigaciones Científicas y Técnicas, Buenos Aires, Argentina. His research interests include condition monitoring and diagnostics of electric machines and drives, electric vehicles, and renewable energy generation. Dr. de la Barrera was Vice-Chair (in 2017), and Chair (in 2018) of the Argentina Section Joint Chapter #1 within the IEEE (IE13/CS23/RA24/IA34/PEL35/VT06).

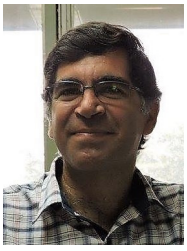

Cristian H. De Angelo (S'96 - M'05 - SM'10) received his Electrical Engineer degree from the Universidad Nacional de Río Cuarto, Argentina, in 1999, and the Dr. of Engineering degree from the Universidad Nacional de La Plata, Argentina, in 2004. In 1994, he joined the Grupo de Electrónica Aplicada, Universidad Nacional de Río Cuarto. He is currently Associate Professor at Universidad Nacional de Río Cuarto and Principal Researcher at Consejo Nacional de Investigaciones Científicas y Técnicas, Argentina. His research interests include electric and hybrid vehicles, fault diagnosis on electric machines, electric motors control, energy efficiency and renewable-energy generation.